JTTEE5 16:698–704
DOI: 10.1007/s11666-007-9102-z
1059-9630/$19.00 © ASM International

Peer Reviewed

Numerical Simulation of Droplet Breakup and Collision in the Solution Precursor Plasma Spraying

Y. Shan, T.W. Coyle, and J. Mostaghimi

(Submitted March 11, 2007; in revised form July 6, 2007)

Finely structured ceramic coatings can be obtained by solution precursor plasma spraying. The final structure of the coating highly depends on the droplet size and velocity distribution at the injection, the evolution of the spray in the jet, and droplet breakup and collision within the spray. This article describes a 3D model to simulate the transport phenomena and the trajectory and heating of the solution spray in the process. O'Rourke's droplet collision model is used to take into account the influence of droplet collision. The influence of droplet breakup is also considered by implementing TAB droplet breakup models into the plasma jet model. The effects of droplet collisions and breakup on the droplet size, velocity, and temperature distribution of the solution spray are investigated. The results indicate that droplet breakup and collision play an important role in determining the final particle size and velocity distributions on the substrate.

Keywords droplet breakup, droplet collision, solution precursor plasma spraying, spray parameters

1. Introduction

The injection of liquid sprays into thermal plasmas has a number of important applications. Examples include thermal plasma chemical vapor deposition (TPCVD), suspension plasma spraying (SPS), and solution precursor plasma spraying (SPPS). The solution precursor plasma spraying is used to generate finely structured ceramic coatings with nano- and sub-micrometric features (Ref 1). In this process, a solution spray of ceramic salts instead ceramic powders is injected into the plasma jet. Rapid heat up and evaporation of the solution droplets result in the formation of the solid particles, which are heated up and accelerated to the substrate to generate the coating. The properties of the coating highly depend on the process parameters, such as the torch operating conditions and the injection parameters of the solution spray (Ref 2). Studies have shown that droplet collision and breakup have important effects on the droplet size distribution of the spray (Ref 3) and also on the dispersion and velocity distribution of the droplets (Ref 4). As a result, droplet collisions and breakup can influence the coating quality of the SPPS. In this article, a 3D model is developed to simulate the solution precursor plasma spraying process. O'Rourke's droplet collision model and Taylor Analogy Breakup (TAB) model are implemented into the model to consider the effect of droplet collision and droplet breakup on the droplet size and velocity distributions of the solution spray.

This article is an invited paper selected from presentations at the 2007 International Thermal Spray Conference and has been expanded from the original presentation. It is simultaneously published in *Global Coating Solutions, Proceedings of the 2007 International Thermal Spray Conference*, Beijing, China, May 14-16, 2007, Basil R. Marple, Margaret M. Hyland, Yuk-Chiu Lau, Chang-Jiu Li, Rogerio S. Lima, and Ghislain Montavon, Ed., ASM International, Materials Park, OH, 2007.

Y. Shan, School of Power Engineering, University of Shanghai for Science and Technology, Shanghai, China; and **T.W. Coyle** and **J. Mostaghimi**, Centre for Advanced Coating Technologies, University of Toronto, Toronto, ON, Canada. Contact e-mail: y.shan@utoronto.ca.

2. Mathematical Models

2.1 Plasma Jet

The following assumptions are made in this model: (1) the flow is time-dependent, incompressible, and turbulent with temperature-dependent properties, (2) the plasma is in local thermodynamic equilibrium and optically thin, (3) the solution is introduced into the jet transversely via a pressure atomizer, and no carrier gas is introduced. On the basis of these assumptions, the time-dependent equations to be solved for the gas phase are conservation of mass, momentum, energy, species, and turbulent kinetic energy and its dissipation. The RNG k-ε model (Ref 5), instead of the standard k-ε model is used to take into account the turbulent characteristics of the plasma jet. The details of this model, and initial and boundary conditions can be found in Ref (6).

2.2 Solution Droplet Evolution

When the solution droplet penetrates into the plasma jet, it is heated up rapidly. Evaporation takes place from

the surface of the droplet. As a result, most of the droplets lose the solvent, and higher concentration solute builds up on the droplet surface. When the droplet temperature reaches its boiling point, the boiling process begins and the solvent moves away from the droplet surface more quickly. With increasing solute concentration in the droplet, saturation level of the solute concentrations is reached, and finally the solution droplet forms a solid particle when all the solvent moves away. Then, those solid particles are heated and accelerated to substrate to produce coatings. Some droplets which are not heated effectively will reach the substrate in a state of liquid solution. These droplets are exposed to high temperature as the jet scans the substrate during the spraying. Evaporation and decomposition of these droplets result in the micro- and nano-size voids that constitute the porosity in the coating microstructure (Ref 7, 8). During the evolution of the solution spray, droplet breakup and collision also occur. To simulate the above physical processes, the temperature within the droplet and the pressure around the droplet are assumed to be uniform, the radiation and rarefaction effects on the droplet are neglected. Since the thermophoretic force is small comparing with the aerodynamic drag force (Ref 9), it is not taken into account in the model. On the basis of these assumptions, Lagrangian equations of motion and heat and mass transfer are used to simulate the droplet behavior in the plasma jet. The details of the evolution of the solution droplet can be found in Ref (6).

2.3 Droplet Collision

When a large number of droplets travel in a flow, there exists a possibility that the droplets may collide. During collisions, droplets may undergo coalescence, grazing, and separation depending on droplets' properties and surrounding gas properties. The droplets collision model used here was developed by O'Rourke (Ref 10). In this model, a binary collision assumption is used, and two types of collisions, coalescence and grazing collisions, are accounted for. To describe the outcomes of droplet collisions, three nondimensional parameters are defined.

The droplet Weber number which compares the inertia to the surface tension forces as follows:

$$We_{\mathrm{d}} = \frac{\rho_{\mathrm{d}} |\vec{v}_1 - \vec{v}_2|^2 r_1}{a(\bar{T}_{\mathrm{d}})} \quad \left(\bar{T}_{\mathrm{d}} = \frac{r_1^3 T_{\mathrm{d}_1} + r_2^3 T_{\mathrm{d}_2}}{r_1^3 + r_2^3} \right) \qquad \text{(Eq 1)}$$

where ρ_{d} and $a(\overline{T_{\mathrm{d}}})$ are the droplet liquid phase specific mass and surface tension, respectively; $\vec{v}_1$ and $\vec{v}_2$ are the velocities of the smaller and larger droplets, respectively. r_1 and r_2 are the radii of the smaller droplet and larger droplet ($r_1 \le r_2$), respectively. T_{d_1} and T_{d_2} are the temperatures of the smaller and larger droplets, respectively.

The droplet size ratio γ:

$$\gamma = \frac{r_2}{r_1}. \qquad \text{(Eq 2)}$$

The dimensionless impact parameter B:

$$B = \frac{b}{r_1 + r_2} \qquad \text{(Eq 3)}$$

where b is the collision impact parameter and is calculated by taking the distance from the center of one droplet to the relative velocity vector placed on the center of the other droplet (Fig. 1). If the impact parameter is less than a critical impact parameter, then the result of every collision is coalescence; if the impact parameter is greater than or equal to a critical impact parameter, then the droplets just graze. The critical impact parameter b_{cr} is given by

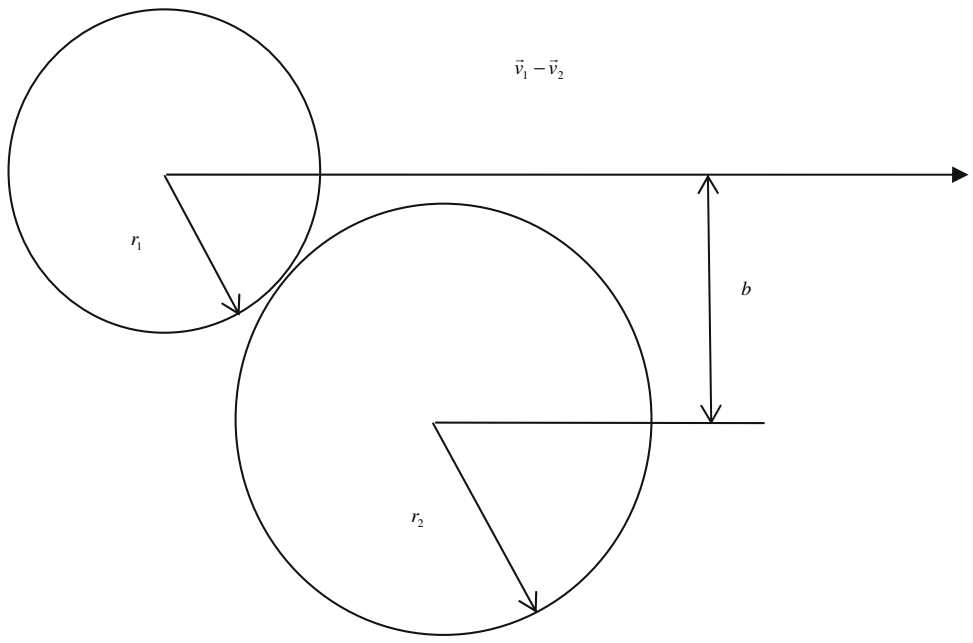

Fig. 1 Definition of impact parameter b

$$b_{cr}^2 = (r_1 + r_2)^2 E_{coal} \quad \text{(Eq 4)}$$

where E_{coal} is the coalescence efficiency, which is defined as the probability of coalescence after the collision. It is expressed as follows:

$$E_{coal} = B^2 = \min\left(1.0, \frac{2.4g(\gamma)}{We_d}\right) \quad \text{(Eq 5)}$$

where the complex function $g(\gamma)$ is approximated by a polynomial for simplicity as follows:

$$g(\gamma) = \gamma^3 - 2.4\gamma^2 + 2.7\gamma \quad \text{(Eq 6)}$$

The discrete droplet parcel approach is used to model the outcomes of droplet collisions. A droplet parcel is assumed to having a certain number of droplets with identical properties. The collision calculation is performed only when two parcels are located in the same computational cell. The collision frequency of one droplet in parcel 2 (larger droplets) with all the droplets in parcel 1 (smaller droplets) is given by

$$I_c = \frac{N_1}{V_c}\pi(r_1 + r_2)^2|\vec{v}_1 - \vec{v}_2|, \quad \text{(Eq 7)}$$

where N_1 is the number of droplets in parcel 1; V_c is the volume of the computational cell that the two parcels occupy. The collision impact parameter b is used to determine the outcome of the collision. If $b < b_{cr}$, then the outcome of every collision is coalescence. The coalescence number n_c for each droplet in parcel 2 is determined by

$$\sum_{k=0}^{n_c-1}\frac{(I_c\Delta t)^k}{k!}e^{-I_c\Delta t} \le XX < \sum_{k=0}^{n_c}\frac{(I_c\Delta t)^k}{k!}e^{-I_c\Delta t}. \quad \text{(Eq 8)}$$

For each droplet in parcel 2, n_c droplets in parcel 1 are subtracted. Then, the size, velocity, and temperature of the coalesced droplets in parcel 2 are modified based on a mass-averaged method.

$$r_2 = \sqrt[3]{r_1^3 + r_2^3} \quad \text{(Eq 9)}$$

$$v_2 = \frac{n_c v_1 r_1^3 + v_2 r_2^3}{r_1^3 + r_2^3} \quad \text{(Eq 10)}$$

$$T_{d_2} = \frac{n_c T_{d_1} r_1^3 + T_{d_2} r_2^3}{r_1^3 + r_2^3}. \quad \text{(Eq 11)}$$

The time step limitation associated with the droplet coalescence calculation is that the computational time step be small compared to the collision time, which is given by

$$\Delta t_c = \frac{V_c}{N_2\pi(r_1 + r_2)^2|\vec{v}_1 - \vec{v}_2|}, \quad \text{(Eq 12)}$$

where N_2 is the number of droplets in parcel 2.

If $b \ge b_{cr}$, the outcome of each collision is a grazing collision. In this case, droplets maintain their sizes and temperatures but undergo velocity changes. The droplet velocities after collisions are given by

$$\vec{v}_1' = \frac{r_1^3\vec{v}_1 + r_2^3\vec{v}_2 + r_2^3(\vec{v}_1 - \vec{v}_2)\frac{b - b_{cr}}{r_1 + r_2 - b_{cr}}}{r_1^3 + r_2^3} \quad \text{(Eq 13)}$$

$$\vec{v}_2' = \frac{r_1^3\vec{v}_1 + r_2^3\vec{v}_2 + r_1^3(\vec{v}_2 - \vec{v}_1)\frac{b - b_{cr}}{r_1 + r_2 - b_{cr}}}{r_1^3 + r_2^3}. \quad \text{(Eq 14)}$$

2.4 Droplet Breakup

2.4.1 TAB Model. This model is based on an analogy between an oscillating and distorting droplet and a spring-mass system (Ref 11). The restoring force of the spring is analogous to the surface tension force. The external force on the mass is analogous to the gas aerodynamic force. The damping force is analogous to the liquid viscous force. Droplet breakup was considered in this model by tracking the value of the distortion y of a droplet. The droplet will experience a breakup if the droplet distortion y exceeds unity. After the breakup, the radii of product droplets are assumed to follow a x-squared distribution:

$$g(r) = \frac{1}{\bar{r}}e^{-r/\bar{r}}, \quad \text{(Eq 15)}$$

where $\bar{r}$ is the number-averaged droplet radius, which is related to the Sauter Mean Radius (SMR) r_{32} by:

$$r_{32} = 3\bar{r} = \frac{r_d}{\frac{7}{3} + \frac{1}{8}\frac{\rho_d r_d^3}{a(T_d)}\dot{y}^2}, \quad \text{(Eq 16)}$$

where $a(T_d)$ is the droplet surface tension coefficient. The product droplet velocities also differ from that of the parent droplet by a velocity with magnitude w_d and with a direction that is randomly distributed in a plane normal to the relative velocity vector between the parent droplet and gas. The quantity w_d is given by

$$w_d = \frac{1}{2}r_d\dot{y}. \quad \text{(Eq 17)}$$

The distortion and oscillation of the droplets are calculated as follows:

$$y = \frac{We}{12} + e^{\frac{t}{t_{dm}}}\left[\left(y_0 - \frac{We}{12}\right)\cos\omega t + \frac{1}{\omega}\left(\dot{y}_0 + \frac{1}{t_{dm}}\left(y_0 - \frac{We}{12}\right)\right)\sin\omega t\right], \quad \text{(Eq 18)}$$

$$\dot{y} = \frac{1}{t_{dm}}\left(\frac{We}{12} - y\right) + e^{\frac{t}{t_{dm}}}\left[\left(\dot{y}_0 + \frac{1}{t_{dm}}\left(y_0 - \frac{We}{12}\right)\right)\cos\omega t - \omega\left(y_0 - \frac{We}{12}\right)\sin\omega t\right], \quad \text{(Eq 19)}$$

where We is the parent droplet Weber number, t_{dm} is the viscous damping time, and ω is the oscillation frequency, which are given as follows:

$$We = \frac{\rho_g|\vec{u} - \vec{v}|^2 r_d}{a(T_d)} \quad \text{(Eq 20)}$$

$$t_{dm} = \frac{2}{5}\frac{\rho_d r_d^2}{\mu_d(T_d)} \quad \text{(Eq 21)}$$

$$\omega^2 = 8\frac{a(T_d)}{\rho_d r_d^3} - \frac{1}{t_{dm}^2}. \quad \text{(Eq 22)}$$

If the droplet is very small or stable, it is possible that $\omega_2 \le 0$. In this case, the distortion y and the distortion rate of change $\dot{y}$ for the next time step is set as zero. If $\omega_2 > 0$, the amplitude A of the undamped oscillation is calculated.

$$A^2 = \left(y - \frac{We}{12}\right)^2 + \left(\frac{\dot{y}}{\omega}\right)^2 \quad \text{(Eq 23)}$$

If $\left(\frac{We}{12} + A\right) \le 1.0$, breakup will not occur. The distortion y and the distortion rate of change $\dot{y}$ for the droplet will be updated using Eq 18 and Eq 19. If $\left(\frac{We}{12} + A\right) > 1.0$, then the breakup time t_b is calculated by assuming that the droplet oscillation is undamped for its first period. This will be true for all except very small droplets. The breakup time t_b is therefore the smallest root greater than the current time step t^n of an undamped version of Eq 18.

$$\frac{We}{12} + A\cos\left[\omega(t - t^n) + \alpha\right] = 1, \quad \text{(Eq 24)}$$

where $\cos\alpha = \frac{y - \frac{We}{12}}{A}$ and $\sin\alpha = -\frac{\dot{y}}{A\omega}$. If $t_b > t^{n+1}$, no breakup occurs on the current time step. The distortion y and the distortion rate of change $\dot{y}$ for the droplet are updated using Eq 18 and 19. If $t_b \le t^{n+1}$, a breakup occurs. The Sauter mean radius (SMR) r_{32} of product droplets is calculated from Eq 16, and the velocity w_d is calculated from Eq 17. The distortion y and the distortion rate of change $\dot{y}$ for the products droplet are set as zero.

2.5 Initial and Boundary Conditions for the Spray Model

At the solution injector exit, droplet size distribution is determined based on the experiment observation (Ref 6). The initial temperature, mass flow rate of the solution spray, oscillating parameters, and injection velocity are specified at the injector exit. The distortion of all injected droplets is assumed to be zero. During the calculation, if a droplet hits a wall, the TRAP boundary condition applies, which terminates the trajectory calculations and records the droplet as ''trapped.'' To simplify the calculation, the entire mass of the droplet is assumed to instantaneously pass into the vapor phase and enter the cell adjacent to the boundary. If a droplet crosses a free boundary or flow boundary, the ESCAPE boundary condition applies, which reports the droplet as having ''escaped'' when it encounters the boundary. Trajectory calculations are terminated.

3. Numerical Technique

Fluent V6.2 code (Ref 5) is used to solve the governing equations of the plasma jet using control volume method and the SIMPLE algorithm of Patankar (Ref 12) with second order upwind scheme. The method used for solving the spray evolution and droplet collision and breakup is based on the ideas of Monte Carlo method and of discrete particle method. The droplet parcels are introduced into the jet during the time of injection. Each parcel is composed of a number of droplets with identical properties. The parcels are sampled randomly from assumed probability distributions that govern droplet properties at injection and droplet collision and breakup behavior after injection. To consider the effect of the heat, mass, and momentum exchange between the spray and the plasma jet, two-way coupling is accomplished by alternately solving the discrete and continuous phase equations until the solutions in both phases have stopped changing.

4. Results and Discussion

4.1 Calculating Conditions

The validity of the plasma jet model is shown in Ref (6). In following sections, a solution spray is injected into the plasma jet. The operating conditions are shown in Table 1. The mass flow rate of the plasma gas is 0.0018 kg/s. The maximum axial velocity and temperature on the centerline at the torch exit are $u_m = 1000$ m/s and $T_m = 11{,}500$ K, respectively. The computational domain is $0.02\ \text{m} \times 2\pi \times 0.08$ mm and divided into $22 \times 50 \times 40$ grids points according to the $(r \times \theta \times z)$ cylindrical coordinate system. The injector locates at the position (0.01 m, 0°, 0.003 m). The diameter of the torch exit is 7.8 mm. The concentration of the solution is 0.5 M. The solvent is water. The final product of the solute is (La0.85Sr0.15)MnO3 (LSM) (specific mass: 6570 kg/m^3, specific heat 573 J/kg K, and melting temperature 2153 K). Initial droplet size distribution is chose based on experiment observation. The minimum droplet diameter is set to 5 μm and the maximum droplet diameter is set to 50 μm. The injection velocity is 20-50 m/s. The initial temperature is 300 K.

4.2 Effect of the Droplet Breakup

In this section, only TAB breakup model is turned on to evaluate the effect of droplet breakup. Figure 2 shows the computed droplet size, axial velocity, and temperature distributions on the substrate without considering droplet collision and breakup. The results in Fig. 2 are set as a base case in following sections. Figure 3 shows the computed droplet size, axial velocity, and temperature distribution on the substrate with considering droplet breakup only. It can be seen that the droplet size decreases due to

Table 1 Operating parameters

Torch current	700 A
Torch voltage	28 V
Ar flow rate	62 slpm
H_2 flow rate	2 slpm
Stand off distance	0.08 m
Solution mass flow rate	0.0002 kg/s

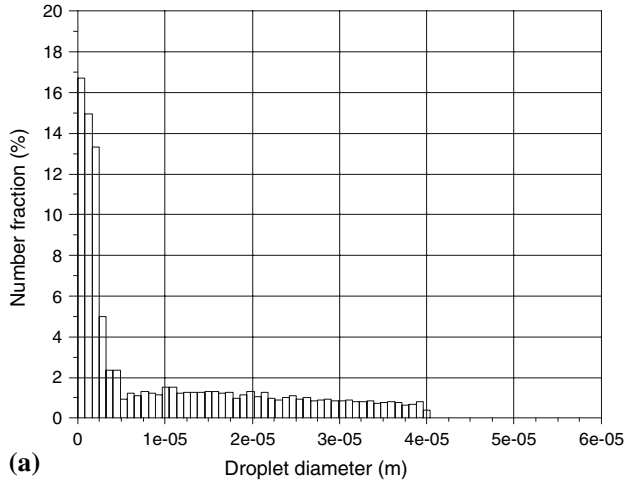

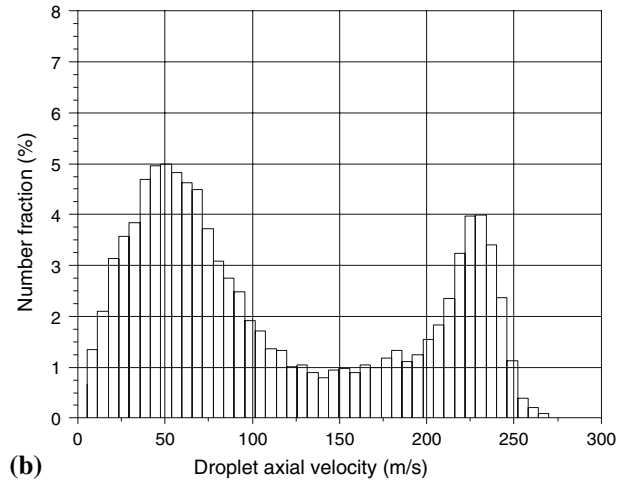

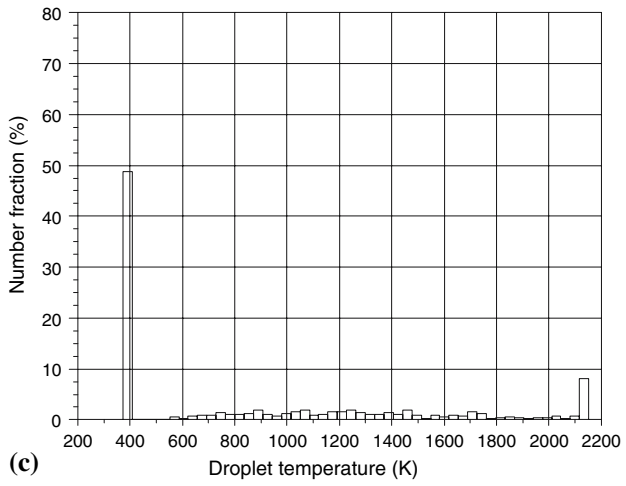

Fig. 2 Computed droplet size (a), axial velocity (b), and temperature (c) distribution on the substrate without considering droplet collision and breakup

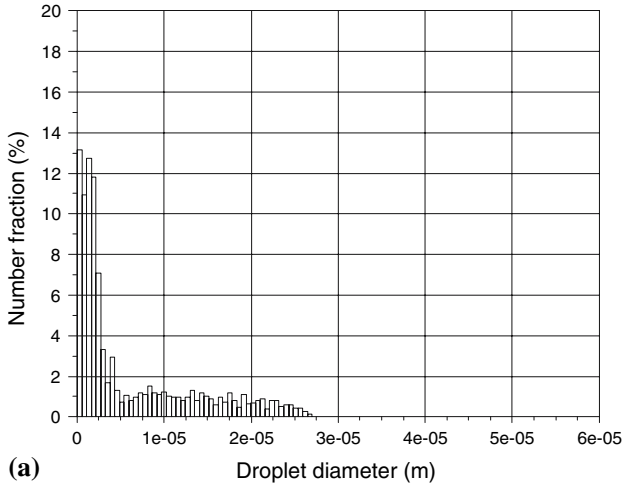

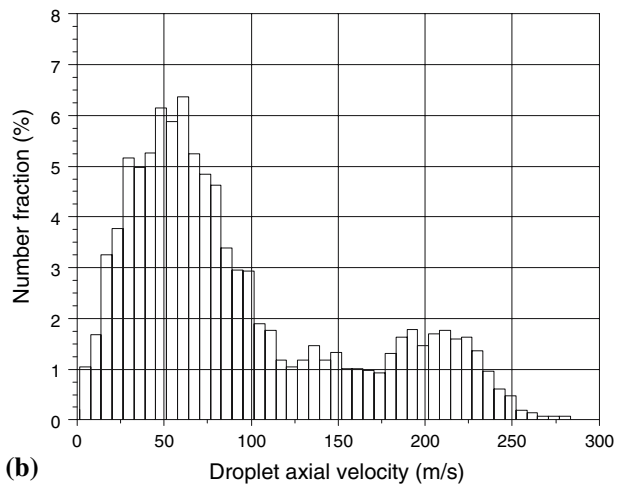

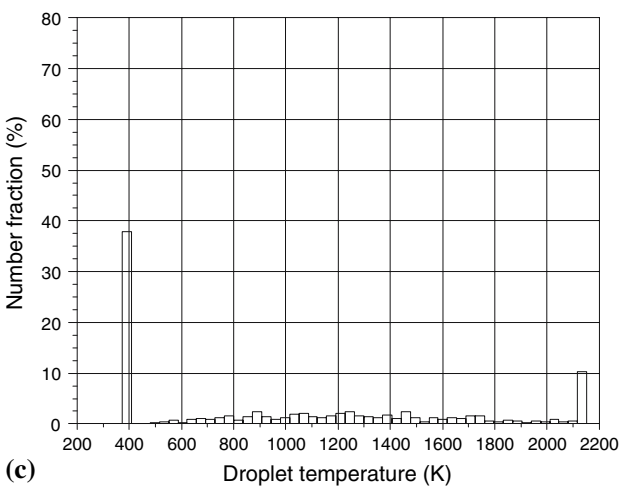

Fig. 3 Computed droplet size (a), axial velocity (b), and temperature (c) distribution on the substrate considering droplet breakup only

the breakup. The mean diameter of the droplet sizes in Fig. 2a is 10.2 μm. In Fig. 3a, the mean diameter of the droplet size is 6.05 μm. Compare the droplet velocity distributions under these two cases, it can be seen that the portion of the droplets with lower velocity increases due to droplet breakup (Fig. 3b). This is because the droplet breakup produces smaller droplets and the smaller droplets accelerated by the plasma jet have low momentum.

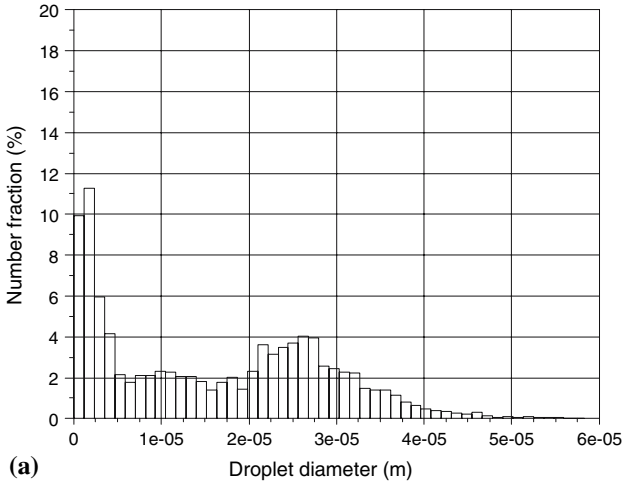

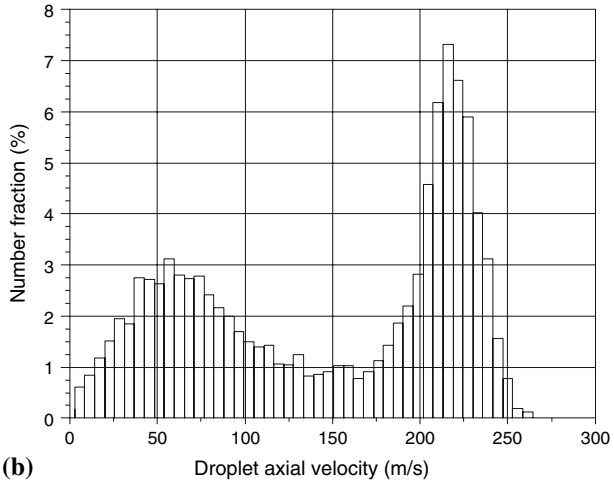

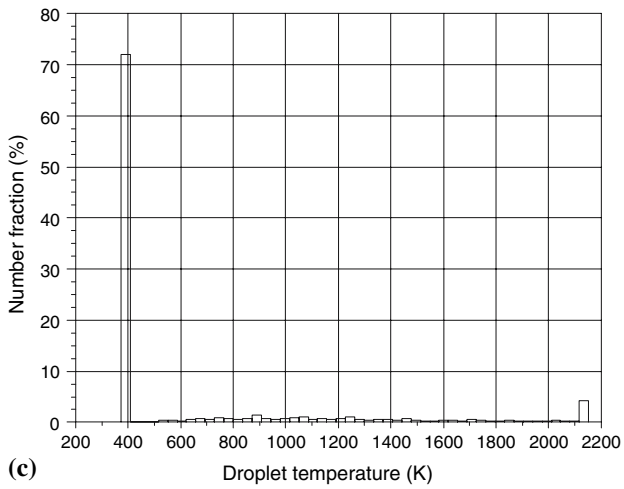

Fig. 4 Computed droplet size (a), axial velocity (b), and temperature (c) distribution on the substrate with considering droplet collision only

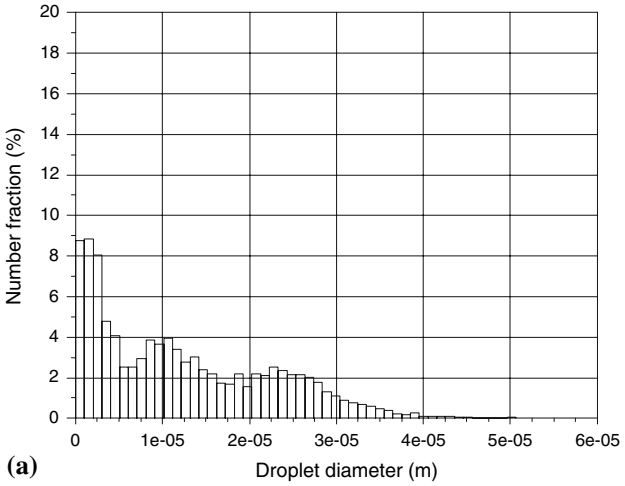

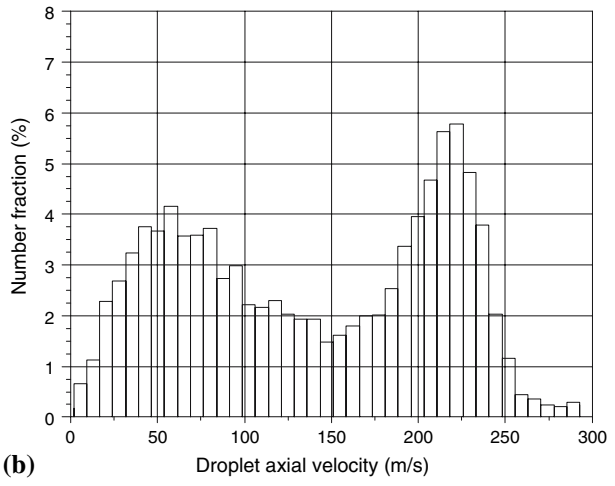

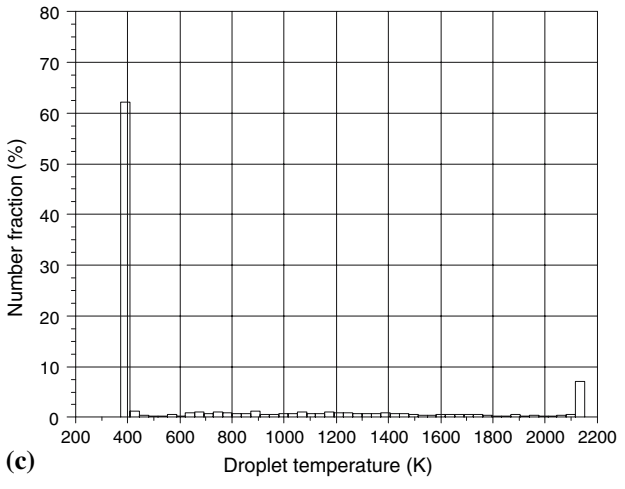

Fig. 5 Computed droplet size (a), axial velocity (b), and temperature (c) distribution on the substrate with considering droplet collision and droplet breakup

When the jet velocity decreases, the smaller droplet cannot remain at its high velocity gained from the upstream of the jet. As a result, the portion of the droplets with lower velocity increases due to droplet breakup. In the temperature distribution figures, the temperature of a large portion of droplets is less than 400 K. This indicates that these droplets arrive on the substrate in a state of liquid solution, and their temperatures remain at the

boiling point of the solvent (water). Since the droplet size decreases due to the breakup, more droplets will completely evaporate and form solid particles. Therefore, the portion of the droplets at boiling temperature decreases and the portion of the solid particles increases (Fig. 3c).

4.3 Effect of the Droplet Collision

In this section, only droplet collision model is turned on to evaluate the effect of droplet collision. Figure 4 shows the computed droplet size, axial velocity and temperature distributions on the substrate considering droplet collision only. It can be seen that the droplet size increases due to the droplet collision (compare Fig. 2a with Fig. 4a). The mean diameter of the droplet sizes in Fig. 4a is 16 μm, which is greater than the one in Fig. 2a. It can be seen that the portion of the droplets with higher velocity increases due to droplet collision. As explained in the previous section, this is because the droplet collision produces bigger droplets, and the bigger droplets accelerated by the plasma jet have high momentum. When the jet velocity decreases downstream, the bigger droplet can remain at its high velocity gained from the upstream of the jet longer than the smaller droplet. Since droplet sizes increase due to droplet collision, the portion of the droplets at boiling temperature increases and the portion of the solid particles decreases (Fig. 4c).

4.4 Combined Effect of the Droplet Collision and Breakup

Figure 5 shows the computed droplet size, axial velocity, and temperature distributions on the substrate with considering both droplet collision and breakup. It can be seen that although some very large droplets are produced due to droplet collision, the average droplet size is less than that of the case considering droplet collision only (the mean diameter in Fig. 5a is 12.2 μm), but it is greater than that of the case considering droplet breakup only. The effect on the droplet velocity and temperature distribution is also in between.

5. Conclusions

A 3D model has been developed to study the solution precursor plasma spraying process. Droplet collision and breakup are considered. The effects of droplet collision and breakup on the droplet size, velocity, and temperature distribution of the solution spray are investigated. It is found that droplet collision increases the average droplet size of the spray, while droplet breakup decreases the average droplet size of the spray. The combined effect of droplet collision and breakup play an important role in determining the final particle size and velocity distributions on the substrate.

Acknowledgments

The financial support of the NSERC of Canada, the National Natural Science Foundation of China (Project 50706027), and the Shanghai Municipal Education Commission (Project 05EZ16) is gratefully acknowledged.

References

1. J. Karthikeyan, C.C. Berndt, S. Reddy, J.Y. Wang, A.H. King, and H. Herman, Nano-material Deposits Formed by DC Plasma Spraying of Liquid Feedstocks, *J. Am. Ceram. Soc.*, 1998, **81**(1), p 121-128
2. N.P. Padture, K.W. Schlichting, T. Bhatia, A. Ozturk B.M. Cetegen, E.H. Jordan, and M. Gell, Towards Durable Thermal Barrier Coatings with Novel Microstructures Deposited by Solution-precursor Plasma Spray, *Acta Mater.*, 2001, **49**(12), p 2251-2257
3. Y. Shan and J. Mostaghimi, Modeling Injection of Dense Liquid Sprays in Radio Frequency Inductively Coupled Plasmas, *Plasma Chem. Plasma Process.*, 2005, **25**(3), p 193-214
4. M. Gavaises, A. Theodorakakos, G. Bergeles, and G. Breen, Evaluation of the Effect of Droplet Collisions on Spray Mixing, *Proc. Institut. Mech. Eng.*, 1996, **210**(5), p 465-475
5. Fluent Inc, *Fluent V6.2 User's Guide*. Lebanon, NH, USA, 2005
6. Y. Shan, T.W. Coyle, and J. Mostaghimi, Numerical Simulation of the Solution Precursor Plasma Spraying Process, *Thermal Spray 2007: Global Coating Solutions*, B.R. Marple, M.M. Hyland, Y.C. Lau, C.J. Li, R.S. Lima, and G. Montavon, Eds., ASM International, Materials Park, Ohio, USA, 2007, p 190-195
7. A. Ozturk and B.M. Cetegen, Modeling of Axially and Transversely Injected Precursor Droplets into a Plasma Environment, *Int. J. Heat Mass Tran.*, 2005, **48**, p 4367-4383
8. L. Xie, E.H. Jordan, N.P. Padture, and M. Gell, Phase and Microstructural Stability of Solution Precursor Plasma Sprayed Thermal Barrier Coatings, *Mater. Sci. Eng. A*, 2004, **381**, p 189-195
9. E. Pfender and Y.C. Lee, Particle Dynamics and Particle Heat and Mass Transfer in Thermal Plasmas—Part I: The Motion of a Single Particle without Thermal Effects, *Plasma Chem. Plasma Process.*, 1985, **5**, p 211-237
10. P.J. O'Rourke, "Collective Drop Effects in Vaporizing Liquid Sprays," Ph.D. Thesis, Princeton University, Princeton, NJ, USA, 1981
11. P.J. O'Rourke and A.A. Amsden, The Tab Method for Numerical Calculation of Spray Droplet Breakup, *SAE Technical Paper* 872089, 1987
12. S.V. Patankar, Numerical Fluid Flow and Heat Transfer. McGraw-Hill, New York, 1980